HHS Public Access

Author manuscript

J Bone Miner Res. Author manuscript; available in PMC 2016 December 01.

Published in final edited form as:

J Bone Miner Res. 2015 December ; 30(12): 2229–2238. doi:10.1002/jbmr.2580.

A Surrogate Measure of Cortical Bone Matrix Density by Long T_2-Suppressed MRI

Alan C. Seifert, B.S.[1], **Cheng Li, Ph.D.**[1], **Suzanne L. Wehrli, Ph.D.**[2], and **Felix W. Wehrli, Ph.D.**[1]

[1]Laboratory for Structural NMR Imaging, Department of Radiology, University of Pennsylvania, Philadelphia, PA

[2]NMR Core Facility, Children's Hospital of Philadelphia, Philadelphia, PA

Abstract

Magnetic resonance has the potential to image and quantify two pools of water within bone: free water within the Haversian pore system (transverse relaxation time, T_2 > 1 ms), and water hydrogen-bonded to matrix collagen (T_2 ~ 300–400 μs). While total bone water concentration quantified by MRI has been shown to scale with porosity, greater insight into bone matrix density and porosity may be gained by relaxation-based separation of bound and pore water fractions. The objective of this study was to evaluate a recently developed surrogate measurement for matrix density, single adiabatic inversion recovery (SIR) zero echo-time (ZTE) MRI, in human bone.

Specimens of tibial cortical bone from 15 donors (27–97 y/o, eight female and seven male) were examined at 9.4T field strength using two methods: (1) ^{1}H ZTE MRI, to capture total ^{1}H signal, and (2) ^{1}H SIR-ZTE MRI, to selectively image matrix-associated ^{1}H signal. Total water, bone matrix, and bone mineral densities were also quantified gravimetrically, and porosity was measured by micro-CT.

ZTE apparent total water ^{1}H concentration was 32.7±3.2 M (range: 28.5–40.3 M), and was correlated positively with porosity (R^2 = 0.80) and negatively with matrix and mineral densities (R^2 = 0.90 and 0.82, respectively). SIR-ZTE apparent bound water ^{1}H concentration was 32.9±3.9 M (range: 24.4–39.8 M), and its correlations were opposite to those of apparent total water: negative with porosity (R^2 = 0.73) and positive with matrix density (R^2 = 0.74) and mineral density (R^2 = 0.72). Porosity was strongly correlated with gravimetric matrix density (R^2 = 0.91, negative) and total water density (R^2 = 0.92, positive). The strong correlations of SIR-ZTE-derived apparent bound water ^{1}H concentration with ground-truth measurements suggest that this quantitative solid-state MRI method provides a nondestructive surrogate measure of bone matrix density.

Corresponding author: Felix W. Wehrli, Ph.D.: wehrli@mail.med.upenn.edu, Address: University of Pennsylvania Medical Center, MRI Education Center, 1st Floor Founders, 3400 Spruce St., Philadelphia, PA 19104, Phone: 215-662-7951, Fax: 215-662-7263.

Disclosures: All authors state that they have no conflicts of interest.

Study design: ACS and FWW. Study conduct: ACS, CL, and SLW. Data collection: ACS. Data analysis: ACS. Data interpretation: ACS, SLW, and FWW. Drafting manuscript: ACS. Revising manuscript content: ACS and FWW. Approving final version of manuscript: ACS, CL, SLW, and FWW. ACS takes responsibility for the integrity of the data analysis.

Keywords

Bone water; MRI; zero echo-time (ZTE); bone density; bone porosity

1. Introduction

Bone is composed of apatite-like mineral, collagen, and water arranged in a complex manner over several size scales[1]. These three components contribute to the tissue's mechanical properties in unique ways: mineral is responsible for bone's compressive strength and rigidity[2], collagen matrix provides tensile strength and elasticity[3], and water serves as a medium for transport of nutrients and is responsible for bone's viscoelasticity[4], a property which increases toughness[5].

Standard clinical assessment of bone health is most commonly performed using dual energy x-ray absorptiometry (DXA), which expresses areal bone mineral density (BMD), or mineral mass per total cross-sectional area of bone, as a T-score relative to that of a young, healthy adult[6]. Though this method is in widespread use, it is insensitive to bone matrix and water content and fails to explain a significant portion of the increased fracture risk that occurs with aging[7]. However, density and hydration state of bone matrix collagen are important determinants of bone quality[8], and measurements of these properties can provide complementary (and potentially superior) information on bone strength[5,9–11].

Over the past decade, various solid-state magnetic resonance imaging (MRI) methods have emerged that allow detection and quantification of bone water, which, due to its short transverse relaxation time (T_2), is invisible to conventional MRI methods. Ultrashort echo time (UTE) MRI has been shown to visualize and quantify the short-T_2 ^{1}H signal of bone water[12–14], and a similar technique, zero echo-time (ZTE) imaging, has also shown promise to detect extremely short-T_2 signals[15–19].

Bone water exists in two major pools that are visible to solid-state MRI: water diffusing freely within the Haversian pore system[20], and water that is hydrogen-bonded to matrix collagen[21–23]. These two pools differ significantly in their ^{1}H nuclear magnetic resonance (NMR) relaxation properties. Pore water has long T_2 > 1 ms at 4.7T, while bound water has T_2 ~ 300–400 μs[21]. A separate ^{1}H NMR signal fraction with extremely short T_2 ~ 60 μs is also visible with specialized spectroscopic hardware, and has been postulated to arise from ^{1}H nuclei in bone matrix collagen. These signal pools are diagrammed in a schematic T_2 spectrum shown in Figure 1.

The aforementioned differences in relaxation properties between bone ^{1}H signal components can be exploited to distinguish the matrix-associated short-T_2 fraction from longer-T_2 signal arising from pore water. MRI of matrix-bound water has been studied by several groups in recent years as a possible surrogate for collagen bone matrix[24–34].

There are two general approaches to pore water suppression taken in prior work: bi-component effective transverse relaxation time (T_2*) fitting of a free-induction decay (FID) or a series of images obtained at multiple echo times (TE)[25,27,28], and T_2-selective

magnetization preparation using either a long, low-amplitude radiofrequency (RF) saturation pulse[24,26,33] or an adiabatic inversion pulse followed by an inversion-recovery delay time (TI)[29–32,34,35].

The major difference between T_2* and T_2, in general, is that T_2* relaxation encompasses all mechanisms responsible for T_2 relaxation, as well as an additional contribution due to magnetic field inhomogeneity on a sub-voxel scale. The large difference in volume magnetic susceptibility (χ_v) between water (χ_v = −8.9 ppm) and bone tissue (χ_v = −11.3 ppm[36]) and the complex arrangement of these two phases in bone leads to strong internal magnetic field gradients within the pore spaces. These gradients cause significant additional attenuation in pore water ^{1}H signal, especially in small pores, reducing the T_2* of pore water nearer to that of bound water[37], whose T_2 and T_2* relaxation are both dominated by dipolar relaxation. The T_2 of pore water remains long, due to rephasing of isochromats by the 180° pulses.

The single adiabatic inversion-recovery (SIR) method, therefore, has the potential to outperform T_2*-based methods of pore water suppression. While duration and bandwidth are inversely proportional in non-adiabatic pulses, they are less strictly linked in adiabatic RF pulses. Such a pulse can therefore simultaneously possess a long duration and broad bandwidth. The long duration allows it to saturate short-T_2 signal while inverting long-T_2 signal, and the broad bandwidth encompasses the broad frequency distribution of pore water within the inhomogeneous internal magnetic field environment of bone pores.

The objective of the present study was to measure zero echo time (ZTE)-derived apparent total water (aTW) and SIR-ZTE-derived apparent bound water (aBW) ^{1}H concentrations in human cortical bone, and to evaluate the hypothesis that aBW ^{1}H concentration parallels bone matrix density and scales inversely with porosity. These concentrations are termed ‘apparent’ in that systematic measurement errors may cause overestimation of true bone water ^{1}H concentration. This work thus may provide a foundation upon which to build a two-part non-invasive in vivo examination of true bone tissue mineralization density (also referred to as ‘degree of mineralization of bone’[38]) consisting of bone matrix and mineral densities by ^{1}H SIR-ZTE and ^{31}P ZTE, respectively. Such an examination could potentially aid in the differentiation of bone-demineralizing disorders from osteoporosis.

2. Materials and Methods

2.1. Specimens and Scanners

The tissue examined consisted of cortical bone specimens taken from the tibial mid-shaft of seven male and eight female human donors, aged 27–97 years (National Disease Research Interchange, NDRI). Specimens were harvested within 30 hours of death and immediately frozen. Time between tissue harvest and this study was 8–11 years. This set ranges from young, dense bone to severely porous bone due to age-related bone loss. Donors with bone-demineralizing disorders were excluded.

A 4-mm slice was sectioned from each thawed tibia with a rotating blade at the region of maximum cortical bone thickness, 38% of the length of the tibia from the medial malleolus to the medial condyle. Then, a rectangular beam with its long axis perpendicular to the

osteonal axis was cut from each slice and trimmed to fit inside a 5-mm NMR tube. Specimens ranged from 15 to 35 mm in length. The direction of the osteonal axis of the bone was indicated on the end of each beam by cutting a notch parallel to the bone's osteonal axis, and specimens were stored individually in phosphate-buffered saline.

All scanning was performed in a 9.4T vertical-bore NMR spectrometer and micro-imaging scanner (Avance III, Bruker, Billerica, MA). For measurement of relaxation times, a broad-band inverse (BBI) probe with a one-axis z-gradient was used, and for imaging, a 20-mm quadrature birdcage probe in a three-axis microimaging gradient set was used. Bones were imaged in the presence of an intensity reference sample consisting of a 20-mm column of 10 mM $MnCl_2$ in 90% D_2O/10% H_2O in a 5-mm NMR tube. This sample had a ^1H concentration of 11.1 M, T_2 = 530 μs, and T_1 = 12.7 ms.

2.2. Measurement of Relaxation Times

Prior to imaging, all bones were scanned using a saturation recovery (SR)-prepared Carr-Purcell-Meiboom-Gill (CPMG) pulse sequence (Figure 2) to measure the T_1, T_2, and T_2* relaxation times of the bound and pore water fractions. Knowledge of these relaxation times is necessary for subsequent conversion of raw MR image intensities to ^1H concentration. The fitting of these SR-CPMG data to bi-exponential functions is illustrated in Figure 3 and described in detail in the Appendix.

2.3. Zero Echo-Time Imaging

Imaging and reconstruction were performed using the standard Bruker ZTE pulse sequence (Figure 4a), and a modified form of this sequence incorporating a single adiabatic inversion preparation and delay time (SIR-ZTE, Figure 4b). ZTE was chosen due to its superior SNR performance to UTE in samples with extremely short T_2*[39]. Gradient amplitude was limited to 73.4 mT/m by two simultaneous requirements of the reconstruction method[40]: (1) that the field of view (FOV) fully enclose all sources of signal, including the plastic support structure of the NMR probe, and (2) that the readout bandwidth be low enough (i.e., that the dwell time be long enough) so as not to lose more than ~2 readout points during the hardware-dependent transmit/receive switching dead time. Due to this finite dead time, the ZTE sequence does not actually acquire signal beginning at TE = 0; the minimum delay time is instead equal to the transmit/receive switching time of 6.4 μs. Though greater than zero, this dead time is negligible for bound and pore water signal having T_2 > 300 μs.

First, each specimen was scanned with the reference sample using ZTE without adiabatic inversion recovery. Then, each specimen was immediately scanned again using SIR-ZTE. The adiabatic inversion pulse, with bandwidth of 5 kHz and duration of 5 ms, selectively saturates the longitudinal magnetization, M_z, of the short-T_2 protons in matrix-bound water (M_z = 0) while inverting long-T_2 signal arising from pore water and marrow fat (M_z < 0)[29,35,41–43]. The T_2 response of M_z to this pulse was calculated by Bloch equation simulation. Following an appropriately chosen inversion-recovery time, the long-T_2 magnetization will be nulled as it passes through zero, and the short-T_2 magnetization will have recovered by longitudinal relaxation to M_z > 0. A ZTE imaging module applied at this time will thus selectively image short-T_2 signal. SIR-ZTE was performed with a repetition

time (TR) of 200 ms and inversion time (TI) of 50 ms, and in both of these sequences, FOV was 64 mm and resolution was 500 μm (both isotropic). Readout bandwidth in both sequences was adequate to render unnecessary any correction for signal loss due to attenuation of high spatial frequencies.

2.4. Density Quantification

To convert raw image intensity to ^{1}H concentration, each image was corrected for longitudinal and transverse relaxation, including transverse relaxation during RF pulses. Each image was imported into Matlab (Mathworks, Natick, MA), and volumes of interest (VOIs) were drawn to fully enclose the bone and the reference sample. Then, within each VOI, the image intensity was corrected by solving Equation 3 for ρ (see Appendix), using the average relaxation times for the set of bone specimens and the measured relaxation times of the reference sample. Next, the bone and reference VOIs were refined by automatic thresholding[44], and, finally, the ^{1}H concentration ($[^1H]$) within the bone was calculated as the ratio of the mean corrected intensity within the bone to that of the reference, multiplied by the known ^{1}H concentration, $[^1H] = 11.1$ M, within the reference sample.

2.5. Micro-CT Imaging

Bone specimens were imaged using a Scanco μCT35 scanner (Scanco, Brüttisellen, Switzerland) at 18.5-μm isotropic voxel resolution. Bone boundaries were masked by 3D active snakes using ITK-SNAP[45]. Pores were then segmented within these bone masks by automated thresholding, and porosity was calculated as pore volume divided by total bone volume.

2.6. Gravimetry

Bone specimens were removed from phosphate-buffered saline, blotted dry, and weighed to determine their fully hydrated mass. The bones were then placed in tared crucibles and dried at 105°C for 110 hr to remove all bound and pore water. Completion of drying was verified by observing no change in mass over a 24-hour period. The bones were again weighed, and their dry mass was recorded. Finally, the bones were incinerated at 600°C for 30 hr to burn off all organic material, and the residue was weighed. Total water mass was calculated as the difference between hydrated and dry masses, matrix mass was the difference between dry and ash masses, and mineral mass was equal to the residual ash mass. These masses were divided by total bone volume (the volume of the μCT bone boundary mask) to yield total water, matrix, and mineral densities[24,46].

3. Results

3.1. Gravimetry and μCT

All bone measurement results, both from MRI and validation methods, are given in Table 1. Mean porosity across the 15 donors was 8.96±8.61% (3.06–33.5%); all data expressed in this format are mean ± standard deviation (min-max). Volume renderings of the pore spaces of four representative bone specimens are shown in Figure 5. Gravimetric mineral density was 1118±130 mg/cc (751–1219 mg/cc), matrix density was 503.7±24.3 mg/cc (437.0–527.5 mg/cc), and total water density was 326.2±48.4 mg/cc (281.4–435.6 mg/cc) bone

tissue (i.e. 32.6% v/v or 36.1 M). The mineralization mass ratio, which is the unitless ratio of gravimetric mineral density to matrix density, was 2.212±0.173 (1.719–2.367), and bone mineralization, which is the bone mineral density normalized by bone volume fraction (1 - porosity), was 1225±36 mg/cc (1130–1286 mg/cc).

Porosity was strongly correlated with gravimetric mineral density (R^2 = 0.98, negative), matrix density (R^2 = 0.91, negative), and total water density (R^2 = 0.92, positive). Matrix and mineral densities were also strongly positively correlated (R^2 = 0.91). The mineralization mass ratio, however, was strongly positively correlated with mineral density (R^2 = 0.96) and negatively correlated with porosity (R^2 = 0.94).

3.2. MRI-Derived Density

ZTE-derived aTW ^{1}H concentration was 32.7±3.2 M (28.5–40.3 M), and SIR-ZTE-derived aBW ^{1}H concentration was 32.9±3.9 M (24.4–39.8 M). MRI quantifies the electromagnetic signal emitted by ^{1}H nuclei within a voxel, so these measurements are properly expressed in molar concentrations of ^{1}H nuclei, rather than mass densities in mg/cc.

^{1}H concentration maps of aTW and aBW in four representative bone specimens are given in Figure 6. As age and porosity increase, aTW increases and aBW decreases. Note especially the region of extreme structural degradation (indicated by white arrows), with high aTW and commensurately lower aBW ^{1}H concentration.

Apparent total water concentration was correlated positively with porosity and gravimetric water density (R^2 = 0.80 and 0.79, respectively), and negatively with matrix density and mineral density (R^2 = 0.90 and 0.82, respectively). Apparent bound water correlations were opposite those of aTW; aBW was correlated negatively with porosity and total water density (R^2 = 0.73 and 0.76, respectively), and positively with matrix density and mineral density (R^2 = 0.74 and 0.72, respectively). Scatter plots of aTW and aBW ^{1}H concentration versus porosity, water density, and organic matrix density are given in Figure 7. All relevant correlation coefficients between parameters are given in Table 2.

3.3. Relaxation Times

The short-T_2 ^{1}H fraction had T_1 = 480±80 ms (320–560 ms), T_2 = 540±150 μs (430–980 μs), T_2* = 400±50 μs (330–520 μs), and accounted for 77.0±9.3% (55.4–86.6%) of total signal by 2D bi-component T_1–T_2 fitting. The long-T_2 fraction had T_1 = 1210±300 ms (880–1910 ms), T_2 = 55000±38000 μs (17000–161000 μs), T_2* = 940±230 μs (600–1540 μs), and accounted for 23.0±9.3% (13.4–44.6%) of the signal.

Short-T_2 fraction by 2D T_1–T_2 bi-component fitting was strongly negatively correlated with aTW (R^2 = 0.86) and strongly positively correlated with aBW (R^2 = 0.86). Short-T_2 fraction was also very strongly correlated with porosity (R^2 = 0.90, negative) and gravimetric matrix density (R^2 = 0.89, positive).

4. Discussion

In this study, we presented non-invasive, non-destructive MRI-based measurements of apparent total and bound water ^{1}H concentrations in human cortical bone, and compared these results to gravimetric bone density measurements and μCT porosity. The strong correlations of aBW with both gravimetric matrix density and μCT porosity support the applicability of this method as a surrogate measurement of bone matrix density. This measurement may later be combined with a previously established ^{31}P MRI-based examination of bone mineral density[24,31] to investigate bone tissue mineralization.

Although aTW is a surrogate for bone porosity[32,47,48], it is not positively associated with the density of bone's collagen matrix; rather, it is representative of the voids within that matrix (i.e. pore volume fraction). On the other hand, aBW is positively correlated with matrix density. It is this positive association that renders aBW a useful surrogate for matrix density, and facilitates its future pairing with a measurement of bone mineral density to create a measurement of bone mineralization; specifically, the ratio of mineral density to aBW.

Apparent total water ^{1}H concentration (32.7±3.2 M, 28.5–40.3 M) in this work is greater than the 24 M[49] and 19.3–31.8 M[47] found in previous ^{1}H UTE work at 3T, but the results are more consistent with the 29–41 M measured more recently by Horch et al.[29] using a 4.7T micro-imaging system. This may be due to the improved abilities of the ZTE pulse sequence and experimental (i.e. non-clinical) hardware to image the shortest-T_2 components in bone. The aTW image likely contains signal not only from water, but also the extremely short-T_2 signal fraction illustrated in Figure 1, which does not appear in UTE images obtained on clinical scanners.

Likewise, the aBW ^{1}H concentration of 32.9±3.9 M (24.4–39.8 M) found in the present study using SIR-ZTE is also higher than the 12–24 M found by Horch et al.[29] or 12–23 M by Manhard et al.[30] using SIR-UTE, but these differences may also be explained by the greater ability of ZTE to capture the shortest-T_2 signal present in bone. Long-range blurring of the extremely short-T_2* signal arising from the plastic body of the RF probe, which appears as an increased (but constant) background signal level, and is more severe in aBW images than aTW due to lower readout gradient strength, also causes an additional systematic error in aBW values not present in aTW. The strengths of the correlations of aBW to porosity and matrix density in the present work, however, are consistent with Horch's reported correlations versus peak stress[29] and CPMG-derived short-T_2 pool fraction[29,30].

4.1. Sensitivity to Relaxation Times

All conversions of image intensity to density in this work were performed using average relaxation times for the set of 15 bone specimens, rather than individually measured relaxation times for each specimen. This ensures that the strengths of the correlations observed between the measured MRI ^{1}H concentrations and reference measurements are translatable to eventual in vivo use, where measurement of relaxation times in each subject

would not be practical. Under this constraint, the correlations of aBW with porosity and matrix density remain strong ($R^2 > 0.7$, $p < 0.00005$).

If the T_1 value used in Equations 3–6 is longer than the true T_1 in the specimen, ^1H concentration will be overestimated. A ±5% deviation in T_1 results in ±3.0% error in calculated aTW and ±5.2% error in aBW. Variation in T_2* will have very little effect on the calculated aTW: the same ±5% error in T_2* results in error of approximately ±0.022%. However, due to the T_2-selectivity of the adiabatic inversion pulse, a ±5% change in T_2 will cause an appreciable error of ±3.8% in aBW.

In Equations 3–5, such errors may artificially amplify the true differences in aTW; greater porosity is associated not only with higher total water content, but also longer T_1 and T_2* due to decreased surface interaction and susceptibility effects in larger pores[49]. Equations 4–6, however, suggest that these same errors may slightly reduce the sensitivity of aBW to true bound water content in the case of perfect long-T_2 suppression, but this possible effect is alleviated by the fact that, while pore water relaxation properties are very strongly affected by bone porosity, bound water relaxation times are relatively constant[21]. Only the stable bound water T_1 and T_2* values are used in quantification.

The assumption of perfect long-T_2 nulling by SIR-ZTE in all specimens, however, is not realistic for a single TI applied to both dense and porous bones. In porous bone, although bound water relaxation times are stable, pore water T_1 and T_2 are longer than in dense bone: T_1 of long-T_2 pore water (T_{1L}) by bi-component 2D T_1–T_2 fitting (see Equation 1) ranges from 880 to 1910 ms, and is positively correlated with porosity ($R^2 = 0.70$, $p < 0.0001$). The long T_2 relaxation time (T_{2L}) ranges from 17 ms to 161 ms and is strongly positively correlated with porosity ($R^2 = 0.91$, $p < 10^{-7}$). These relaxation times vary because free water near the surface of a pore experiences an additional contribution to its transverse ($1/T_2$) and longitudinal ($1/T_1$) relaxation rates due to interaction with the surface, typically termed surface relaxation[20]. The contribution of surface relaxation to the relaxation times of the entire pore water pool, therefore, scales with the surface to volume ratio (S/V) of the pore spaces. In very porous bones, cortical pores are large and the S/V ratio is small; however, in young, dense bone, cortical pores are very small and the S/V ratio is large, leading to an increased effect of surface relaxation and more rapid transverse and longitudinal relaxation.

In empirically choosing TI for a set of specimens such that pore water is nulled, TI is biased toward optimal nulling of pore water in more porous bones; these bones have more pore water to be nulled, so proper inversion is more important. In dense bones, with shorter T_{1L} and T_{2L}, pore water magnetization may be incompletely inverted during the adiabatic inversion pulse (i.e., $M_z > -1$) due to transverse relaxation during the pulse, and will undergo significantly faster longitudinal relaxation after inversion, thus overshooting the null point ($M_z > 0$) during the inversion-recovery delay. Some of this pore water magnetization in dense bone will therefore also be imaged, along with bound water magnetization, by SIR-ZTE. This additional contribution of pore water in dense bones is partially responsible for the overestimation of bound water density (which is 60–80% of total bone water[21,22]) by SIR-ZTE, causing average aBW ^1H concentration (32.9±3.9 M,

24.4–39.8 M) to be slightly greater than average aTW (32.7±3.2 M, 28.5–40.3 M). This overestimation, however, does not diminish the strength of the positive correlation of aBW with bone matrix density, or the negative correlation with porosity. In fact, this phenomenon may enhance the sensitivity of aBW to changes in matrix density and porosity. The remainder of this overestimation is due to the previously discussed signal contributed by the plastic body of the RF probe. This issue could be remedied by using proton-free polymers for coil construction.

4.2. Bone Mineralization

The strong positive correlation ($R^2 = 0.91$) between matrix and mineral densities measured by gravimetry confirms that the degree of mineralization in these bones is not the primary determinant of bulk bone mineral density; changes in mineral density are primarily a result of structural degradation rather than a deficit of mineralization. The mineralization mass ratio, which is defined as gravimetric mineral density divided by matrix density, however, was strongly negatively correlated with porosity ($R^2 = 0.94$), consistent with the notion that bone mineralization is decreased due to rapid bone turnover in age-related bone loss.

Tissue mineralization density calculated in this work, 1225±36 mg/cc matrix (1130–1286 mg/cc matrix), was similar to previous microradiographic measurements by Boivin et al.[50] (1082±17 mg/cc). Gravimetric densities are also consistent with gravimetric measurements performed by Cao et al.[24] in rat bone.

4.3. Translatability to the Clinic

This work has established aBW ^{1}H concentration as a surrogate for matrix density. This examination, in combination with a ^{31}P ZTE examination of bone mineral density[31], could be developed into a non-invasive in vivo MRI assessment of bone mineral and matrix densities, and their ratio, the degree of mineralization of bone. If reduced to practice, this MRI method would allow clinicians to discriminate between age-related macroscopic bone loss and impairment of bone mineralization. Such an examination is not possible using standard x-ray-based screening methods.

This study benefitted from the enhanced performance of experimental versus clinical hardware. The 9.4T scanner used in this work is equipped with much stronger gradients than clinical scanners, narrowing the point spread function and, thus, reducing blurring. This allows for better delineation of bone margins, and even enables visualization of individual pore spaces in severely porous bones (see Figure 5, panel 83F). The use of a 20-mm RF probe and very high field strength also yields higher SNR than is achievable using clinical hardware.

Although the maximum achievable gradient strength is limited on clinical scanners, and image blurring due to signal decay during readout will be increased, this issue will be mitigated by the larger size of bones in human subjects compared to the small specimens studied in this work, and the longer T_2* of both bound and pore water at lower B_0. In previous work using these methods at 3T[31], point-spread function blurring was minimal. Also, at clinically relevant field strengths, such as 3T, the difference in T_1 between the bound and pore water signal components is much greater (145 ms and 880 ms, respectively,

at 3T, versus 480 ms and 1210 ms at 9.4T)[37], so the bound water selectivity of the SIR-ZTE method would be enhanced.

5. Conclusion

Based on the strong correlations of aBW ^{1}H concentration with gravimetric matrix density and porosity, long T_2-suppressed solid-state MRI is a promising surrogate for bone matrix density.

Acknowledgements

This work was supported by NIH R01 AR50068, NIH F31 AG042289 (A.C.S.), the Howard Hughes Medical Institute International Student Research Fellowship (C.L.), and the University of Pennsylvania Institute for Translational Medicine and Therapeutics. This work was also supported in part by the National Center for Research Resources Grant UL1RR024134, which is now the National Center for Advancing Translational Sciences Grant UL1TR000003. The content is solely the responsibility of the authors and does not necessarily represent the official views of the NIH.

We also thank Dr. Wei-Ju Tseng for assistance with μCT imaging protocol refinement, and Dr. Steven Szewczyk for facilitating the use of high-temperature furnaces for gravimetric validation.

Appendix

7.1. Measurement of Relaxation Times

Saturation recovery times (T_{SR}) in the SR-CPMG sequence (Figure 2) were arrayed logarithmically in 12 steps from 3 ms to 6 s, and the number of refocusing pulses, N, was arrayed logarithmically from 0 to 5000 in 20 steps, resulting in TEs ranging from zero to 1 s, although the 9-μs transmit/receive dead time must be added to the beginning of each sampled echo. The duration of the refocusing RF pulse, 40 μs, is one order of magnitude less than the shortest relevant T_2 relaxation time, so no corrections for incomplete refocusing are necessary. One signal acquisition was performed, and scan time for this sequence was 29 minutes. All other relevant pulse sequence parameters are given within the pulse sequence diagram in Figure 2.

Two-dimensional bi-component T_1–T_2 fitting was performed by fitting a sum of two exponential functions in two dimensions,

$$f(T_{SR},TE)=M_S(1-e^{\frac{-T_{SR}}{T_{1S}}})e^{\frac{-TE}{T_{2S}}}+M_L(1-e^{\frac{-T_{SR}}{T_{1L}}})e^{\frac{-TE}{T_{2L}}}+n, \quad [1]$$

to the array of SR-CPMG echo amplitudes. Here, the magnetizations of the short- and long-T_2 components are given by M_S and M_L, respectively. These terms are converted to short- and long-T_2 fractions by dividing by their sum, i.e. $M_S/(M_S+M_L)$ and $M_L/(M_S+M_L)$. Longitudinal (T_1) relaxation times are given by T_{1S} and T_{1L}, T_2 relaxation times by T_{2S} and T_{2L}, and the noise level by n. This fitting process yields the sizes of each of the two pools and their characteristic T_1 and T_2 relaxation times.

T_2* values for the pools were also obtained by fitting a similar equation,

$$f(TE,t)=M_S e^{\frac{-TE}{T_{2S}}} e^{\frac{-t}{T^*_{2S}}}+M_L e^{\frac{-TE}{T_{2L}}} e^{\frac{-t}{T^*_{2L}}}+n, \quad [2]$$

to the two-dimensional array of FIDs beginning at the center of each CPMG echo. Here, t is the time within the FID after each echo. These data were taken from the SR-CPMG data set after the longest T_{SR} of 6 seconds, which satisfies the condition of full longitudinal relaxation. This process yields two pools characterized by T_2 and T_2* relaxation times, rather than T_1 and T_2. Fitting was performed in two dimensions, rather than one, for improved accuracy and stability[51]. All fitting was performed in Matlab (Mathworks, Natick, MA). Example data from bone from a 53-year-old male donor, along with bi-component fits, are shown in Figure 3.

7.2. Density Quantification

The steady-state signal acquired in the ZTE sequence (Figure 4a) is given in Equation 3:

$$S(\vec{r}) \propto \rho(\vec{r})\frac{1-\exp(-TR/T_1)}{1-f_z\exp(-TR/T_1)} f_{xy}\exp(-TE/T_2^*), \quad [3]$$

where ρ is aTW ^{1}H concentration. Because ZTE measures total water signal, single-component exponential fitting of SR-CPMG data was performed to determine total water T_1, T_2, and T_2* relaxation times, which were then incorporated into this equation. Also, $e^{-TE/T2^*} \approx 1$ because this pulse sequence has an echo time of approximately zero. The f_{xy} and f_z terms represent the response of the transverse and longitudinal magnetization, respectively, to rectangular RF pulses in the general case, where the pulse is not infinitesimally short relative to T_2*[52]:

$$f_{xy}=\exp(-\tau/2T_2)\alpha\mathrm{sinc}\left(\sqrt{\alpha^2-(\tau/2T_2)^2}\right) \quad [4]$$

and

$$f_z=\exp(-\tau/2T_2)\left[\cos\left(\sqrt{\alpha^2-(\tau/2T_2)^2}\right)+(\tau/2T_2)\mathrm{sinc}\left(\sqrt{\alpha^2-(\tau/2T_2)^2}\right)\right], \quad [5]$$

where τ is RF pulse duration and $\alpha = \gamma B_1 \tau$ is the nominal flip angle.

Quantification of aBW ^{1}H concentration in the SIR-ZTE images is similar, except for three important differences. First, the contribution of the adiabatic inversion pulse was added to Equation 3:

$$S(\vec{r}) \propto \rho(\vec{r})\frac{1+(f_{HS}-1)\exp(-TI/T_1)-f_{HS}\exp(-TR/T_1)}{1-f_{HS}f_z\exp(-TR/T_1)} f_{xy}\exp(-TE/T_2^*), \quad [6]$$

where f_{HS}, the response of the longitudinal magnetization to the adiabatic inversion pulse, was calculated for the bone and reference by Bloch equation simulation based on their respective relaxation times. Also, because long-T_2 signal is nulled in SIR-ZTE, the short T_1, T_2, and T_2* relaxation times measured by bi-component fitting of SR-CPMG data were used

in Equation 6 for relaxation correction, rather than the single-component relaxation times used in Equation 3. Finally, to maintain consistency, the VOIs obtained by automatic thresholding in the ZTE images were carried over for SIR-ZTE correction. Apart from these two changes, quantification of aBW is performed in the same manner as aTW.

References

1. Rho JY, Kuhn-Spearing L, Zioupos P. Mechanical properties and the hierarchical structure of bone. Medical Engineering & Physics. 1998 Mar; 20(2):92–102. [PubMed: 9679227]
2. Glimcher MJ, Bonar LC, Grynpas MD, Landis WJ, Roufosse AH. Recent Studies of Bone Mineral: Is the Amorphous Calcium Phosphate Theory Valid? Journal of Crystal Growth. 1981; 53(1):100–119.
3. Mehta SS, Oz OK, Antich PP. Bone elasticity and ultrasound velocity are affected by subtle changes in the organic matrix. J Bone Miner Res. 1998 Jan; 13(1):114–121. [PubMed: 9443797]
4. Garner E, Lakes R, Lee T, Swan C, Brand R. Viscoelastic dissipation in compact bone: implications for stress-induced fluid flow in bone. J Biomech Eng. 2000 Apr; 122(2):166–172. [PubMed: 10834157]
5. Nyman, JS.; Gorochow, LE.; Horch, RA.; Uppuganti, S.; Zein-Sabatto, A.; Manhard, MK.; Does, MD. Journal of the Mechanical Behavior of Biomedical Materials. Vol. 22. Elsevier; 2013 Jun 1. Partial removal of pore and loosely bound water by low-energy drying decreases cortical bone toughness in young and old donors; p. 136-145.
6. World Health Organization. Geneva: World Health Organ Tech Rep Ser.; 2003. Prevention and management of osteoporosis; p. 1-164.
7. Kanis, JA.; Johnell, O.; Oden, A.; Dawson, A.; De Laet, C.; Jonsson, B. Osteoporos Int. Vol. 12. Springer-Verlag London Limited; 2001. Ten year probabilities of osteoporotic fractures according to BMD and diagnostic thresholds; p. 989-995.
8. Paschalis EP, Mendelsohn R, Boskey AL. Infrared Assessment of Bone Quality: A Review. Clin Orthop Relat Res. 2011 Jan 6; 469(8):2170–2178. [PubMed: 21210314]
9. Unal, M.; Yang, S.; Akkus, O. Bone. Vol. 67. Elsevier; 2014 Oct. Molecular spectroscopic identification of the water compartments in bone; p. 228-236.
10. Samuel, J.; Sinha, D.; Zhao, JC-G.; Wang, X. Bone. Vol. 59. Elsevier Inc; 2014 Feb 1. Water residing in small ultrastructural spaces plays a critical role in the mechanical behavior of bone; p. 199-206.
11. Horch, RA.; Gochberg, DF.; Nyman, JS.; Does, MD. Non-invasive Predictors of Human Cortical Bone Mechanical Properties: T2-Discriminated 1H NMR Compared with High Resolution X-ray. In: Phillips, S., editor. PLoS ONE. Vol. 6. 2011 Jan 21. p. e16359
12. Robson MD, Gatehouse PD, Bydder M, Bydder GM. Magnetic resonance: An introduction to ultrashort TE (UTE) imaging. J Comput Assist Tomogr. 2003; 27(6):825–846. [PubMed: 14600447]
13. Reichert ILH, Robson MD, Gatehouse PD, He T, Chappell KE, Holmes J, Girgis S, Bydder GM. Magnetic resonance imaging of cortical bone with ultrashort TE pulse sequences. Magnetic Resonance Imaging. 2005 Jun; 23(5):611–618. [PubMed: 16051035]
14. Fernández-Seara MA, Wehrli SL, Takahashi M, Wehrli FW. Water Content Measured by Proton-Deuteron Exchange NMR Predicts Bone Mineral Density and Mechanical Properties. J Bone Miner Res. 2003 Dec 16; 19(2):289–296. [PubMed: 14969399]
15. Ackerman JL, Raleigh DP, Glimcher MJ. Phosphorus-31 magnetic resonance imaging of hydroxyapatite: a model for bone imaging. Magn. Reson. Med. 1992 May; 25(1):1–11. [PubMed: 1317501]
16. Wu, Y.; Ackerman, JL.; Chesler, DA.; Li, J.; Neer, RM.; Wang, J.; Glimcher, MJ. Calcified Tissue International. Vol. 62. Springer-Verlag; 1998 Jun. Evaluation of bone mineral density using three-dimensional solid state phosphorus-31 NMR projection imaging; p. 512-518.
17. Hafner S. Fast Imaging in Liquids and Solids with the Back-Projection Low-Angle Shot (Blast) Technique. Magnetic Resonance Imaging. 1994; 12(7):1047–1051. [PubMed: 7997092]

18. Kuethe DO, Caprihan A, Fukushima E, Waggoner RA. Imaging lungs using inert fluorinated gases. Magn. Reson. Med. 1998 Jan; 39(1):85–88. [PubMed: 9438441]
19. Madio, DP.; Lowe, IJ. Magn. Reson. Med. Vol. 34. Wiley Subscription Services, Inc., A Wiley Company; 1995 Oct. Ultra-Fast Imaging Using Low Flip Angles and Fids; p. 525-529.
20. Wang, XD.; Ni, QW. Journal of Orthopaedic Research. Vol. 21. Wiley Subscription Services, Inc., A Wiley Company; 2003 Mar. Determination of cortical bone porosity and pore size distribution using a low field pulsed NMR approach; p. 312-319.
21. Horch RA, Nyman JS, Gochberg DF, Dortch RD, Does MD. Characterization of 1H NMR signal in human cortical bone for magnetic resonance imaging. Magn. Reson. Med. 2010 Aug 25; 64(3): 680–687. [PubMed: 20806375]
22. Ong HH, Wright AC, Wehrli FW. Deuterium nuclear magnetic resonance unambiguously quantifies pore and collagen-bound water in cortical bone. J Bone Miner Res. 2012 Nov 19; 27(12):2573–2581. [PubMed: 22807107]
23. Ni Q, Nyman JS, Wang X, Santos ADL, Nicolella DP. Assessment of water distribution changes in human cortical bone by nuclear magnetic resonance. Meas. Sci. Technol. 2007 Jan 24; 18(3):715–723.
24. Cao, H.; Nazarian, A.; Ackerman, JL.; Snyder, BD.; Rosenberg, AE.; Nazarian, RM.; Hrovat, MI.; Dai, G.; Mintzopoulos, D.; Wu, Y. Bone. Vol. 46. Elsevier Inc; 2010 Jun 1. Quantitative 31P NMR spectroscopy and 1H MRI measurements of bone mineral and matrix density differentiate metabolic bone diseases in rat models; p. 1582-1590.
25. Du J, Diaz E, Carl M, Bae W, Chung CB, Bydder GM. Ultrashort echo time imaging with bicomponent analysis. Magn. Reson. Med. 2011 Oct 27; 67(3):645–649. [PubMed: 22034242]
26. Cao H, Ackerman JL, Hrovat MI, Graham L, Glimcher MJ, Wu Y. Quantitative bone matrix density measurement by water- and fat-suppressed proton projection MRI (WASPI) with polymer calibration phantoms. Magn. Reson. Med. 2008 Dec; 60(6):1433–1443. [PubMed: 19025909]
27. Diaz E, Chung CB, Bae WC, Statum S, Znamirowski R, Bydder GM, Du J. Ultrashort echo time spectroscopic imaging (UTESI): an efficient method for quantifying bound and free water. NMR Biomed. 2011 Jul 15; 25(1):161–168. [PubMed: 21766381]
28. Biswas, R.; Bae, W.; Diaz, E.; Masuda, K.; Chung, CB.; Bydder, GM.; Du, J. Bone. Vol. 50. Elsevier Inc; 2012 Mar 1. Ultrashort echo time (UTE) imaging with bi-component analysis: Bound and free water evaluation of bovine cortical bone subject to sequential drying; p. 749-755.
29. Horch RA, Gochberg DF, Nyman JS, Does MD. Clinically compatible MRI strategies for discriminating bound and pore water in cortical bone. Magn. Reson. Med. 2012 Jan 31; 68(6): 1774–1784. [PubMed: 22294340]
30. Manhard MK, Horch RA, Harkins KD, Gochberg DF, Nyman JS, Does MD. Validation of quantitative bound- and pore-water imaging in cortical bone. Magn. Reson. Med. 2014 Jun; 71(6): 2166–2171. [PubMed: 23878027]
31. Seifert AC, Li C, Rajapakse CS, Bashoor-Zadeh M, Bhagat YA, Wright AC, Zemel BS, Zavaliangos A, Wehrli FW. Bone mineral 31P and matrix-bound water densities measured by solid-state 31P and 1H MRI. NMR Biomed. 2014 Jul; 27(7):739–748. [PubMed: 24846186]
32. Li C, Seifert AC, Rad HS, Bhagat YA, Rajapakse CS, Sun W, Lam SCB, Wehrli FW. Cortical bone water concentration: dependence of MR imaging measures on age and pore volume fraction. Radiology. 2014 Sep; 272(3):796–806. [PubMed: 24814179]
33. Wu Y, Ackerman JL, Chesler DA, Graham L, Wang Y, Glimcher MJ. Density of organic matrix of native mineralized bone measured by water- and fat-suppressed proton projection MRI. Magn. Reson. Med. 2003 Jun 13; 50(1):59–68. [PubMed: 12815679]
34. Du J, Carl M, Bydder M, Takahashi A, Chung CB, Bydder GM. Qualitative and quantitative ultrashort echo time (UTE) imaging of cortical bone. J. Magn. Reson. 2010 Dec; 207(2):304–311. [PubMed: 20980179]
35. Larson PEZ, Conolly SM, Pauly JM, Nishimura DG. Using adiabatic inversion pulses for long-T2 suppression in ultrashort echo time (UTE) imaging. Magn. Reson. Med. 2007; 58(5):952–961. [PubMed: 17969119]

36. Hopkins JA, Wehrli FW. Magnetic susceptibility measurement of insoluble solids by NMR: magnetic susceptibility of bone. Magn. Reson. Med. 1997 Apr; 37(4):494–500. [PubMed: 9094070]
37. Seifert AC, Wehrli SL, Wehrli FW. Bi-component T2* analysis of bound and pore bone water fractions fails at high field strengths. NMR Biomed. 2015 May 18.:n/a–n/a.
38. Boivin G, Meunier PJ. The mineralization of bone tissue: a forgotten dimension in osteoporosis research. Osteoporos Int. 2003; 14(Suppl 3):S19–S24. [PubMed: 12730799]
39. Seifert AC, Wright AC, Wehrli SL, Ong HH, Li C, Wehrli FW. 31P NMR relaxation of cortical bone mineral at multiple magnetic field strengths and levels of demineralization. NMR Biomed. 2013 Mar 18; 26(9):1158–1166. [PubMed: 23505120]
40. Kuethe DO, Caprihan A, Lowe IJ, Madio DP, Gach HM. Transforming NMR data despite missing points. Journal of Magnetic Resonance. 1999 Jul; 139(1):18–25. [PubMed: 10388580]
41. Li C, Magland JF, Rad HS, Song HK, Wehrli FW. Comparison of optimized soft-tissue suppression schemes for ultrashort echo time MRI. Magn. Reson. Med. 2011 Dec 8; 68(3):680–689. [PubMed: 22161636]
42. Du, J.; Bydder, M.; Takahashi, AM.; Carl, M.; Chung, CB.; Bydder, GM. Magnetic Resonance Imaging. Vol. 29. Elsevier Inc; 2011 May 1. Short T2 contrast with three-dimensional ultrashort echo time imaging; p. 470-482.
43. Norris DG, Lüdemann H, Leibfritz D. An analysis of the effects of short T2 values on the hyperbolic-secant pulse. Journal of Magnetic Resonance. 1991; 92(1):94–101.
44. Otsu N. Threshold Selection Method From Gray-Level Histograms. IEEE Transactions on Systems Man and Cybernetics. 1979; 9(1):62–66.
45. Yushkevich PA, Piven J, Hazlett HC, Smith RG, Ho S, Gee JC, Gerig G. User-guided 3D active contour segmentation of anatomical structures: Significantly improved efficiency and reliability. NeuroImage. 2006 Jul; 31(3):1116–1128. [PubMed: 16545965]
46. Anumula S, Magland J, Wehrli SL, Ong H, Song HK, Wehrli FW. Multi-modality study of the compositional and mechanical implications of hypomineralization in a rabbit model of osteomalacia. Bone. 2008 Feb; 42(2):405–413. [PubMed: 18053788]
47. Techawiboonwong A, Song HK, Leonard MB, Wehrli FW. Cortical bone water: in vivo quantification with ultrashort echo-time MR imaging. Radiology. 2008 Sep; 248(3):824–833. [PubMed: 18632530]
48. Techawiboonwong A, Song HK, Wehrli FW. In vivo MRI of submillisecond T(2) species with two-dimensional and three-dimensional radial sequences and applications to the measurement of cortical bone water. NMR Biomed. 2008 Jan; 21(1):59–70. [PubMed: 17506113]
49. Rad HS, Lam SCB, Magland JF, Ong H, Li C, Song HK, Love J, Wehrli FW. Quantifying cortical bone water in vivo by three-dimensional ultra-short echo-time MRI. NMR Biomed. 2011 Jan 28; 24(7):855–864. [PubMed: 21274960]
50. Boivin G, Meunier PJ. The Degree of Mineralization of Bone Tissue Measured by Computerized Quantitative Contact Microradiography. Calcified Tissue International. 2002 May 27; 70(6):503–511. [PubMed: 12019458]
51. Celik H, Bouhrara M, Reiter DA, Fishbein KW, Spencer RG. Stabilization of the inverse Laplace transform of multiexponential decay through introduction of a second dimension. J. Magn. Reson. 2013 Nov.236:134–139. [PubMed: 24035004]
52. Sussman, MS.; Pauly, JM.; Wright, GA. Magn. Reson. Med. Vol. 40. Wiley Subscription Services, Inc., A Wiley Company; 1998. Design of practical T2-selective RF excitation (TELEX) pulses; p. 890-899.

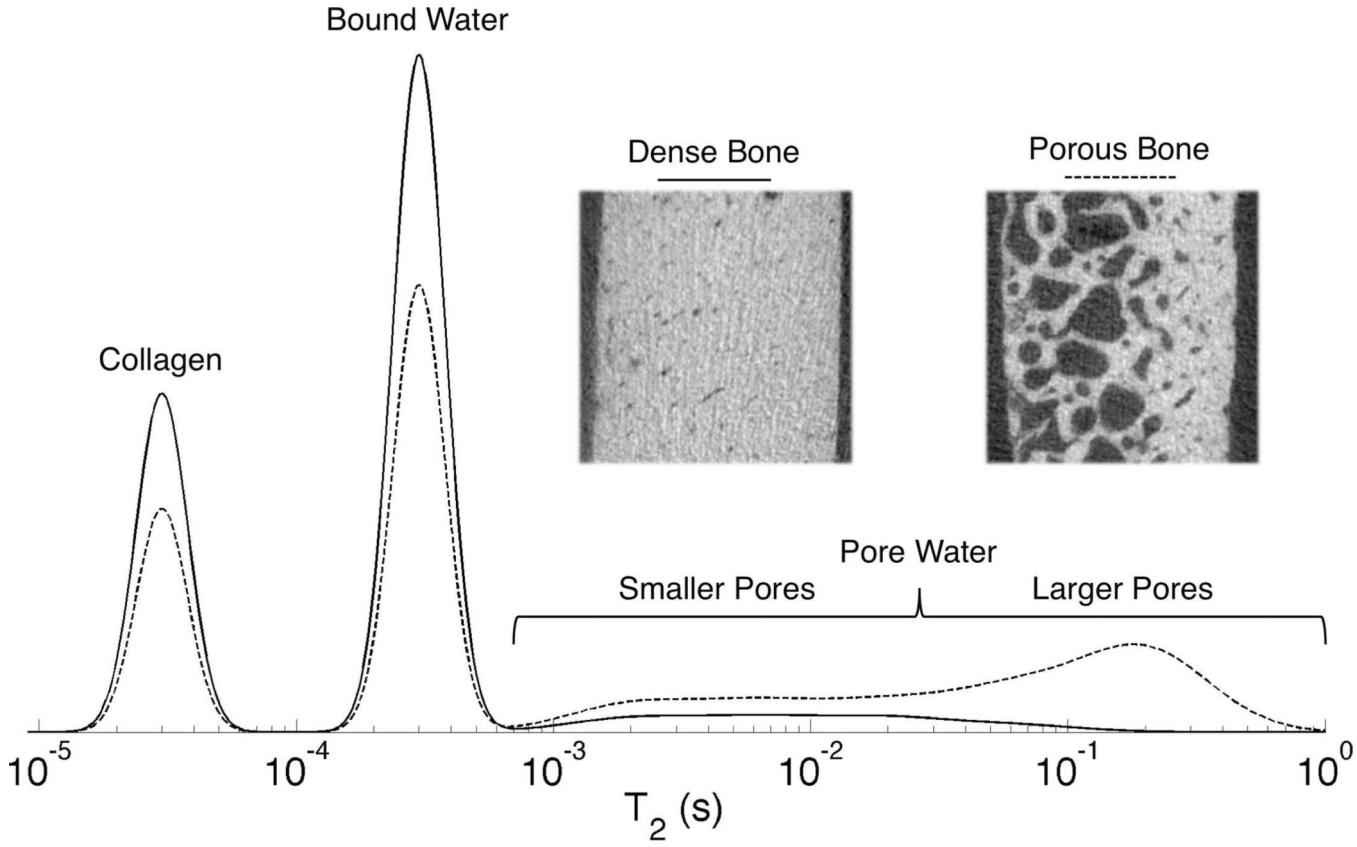

Figure 1.

Schematic T_2 relaxation spectrum diagramming the three major ^{1}H NMR signal pools in bone. Pore water has $T_2 > 1$ ms and is broadly distributed, while bound water has $T_2 \sim 300–500$ μs. Collagen and macromolecular signal, at $T_2 \sim 40–60$ μs, is below the detection limit at clinical field strengths, but becomes visible using micro-imaging and spectroscopic hardware. As porosity increases, as shown in the inset μCT images of bone specimens from 27 y/o and 83 y/o female donors (dense and porous bone, respectively) collagen and bound water content decrease while pore water content increases and shifts to longer T_2 values due the smaller surface-to-volume ratio of enlarged pores.

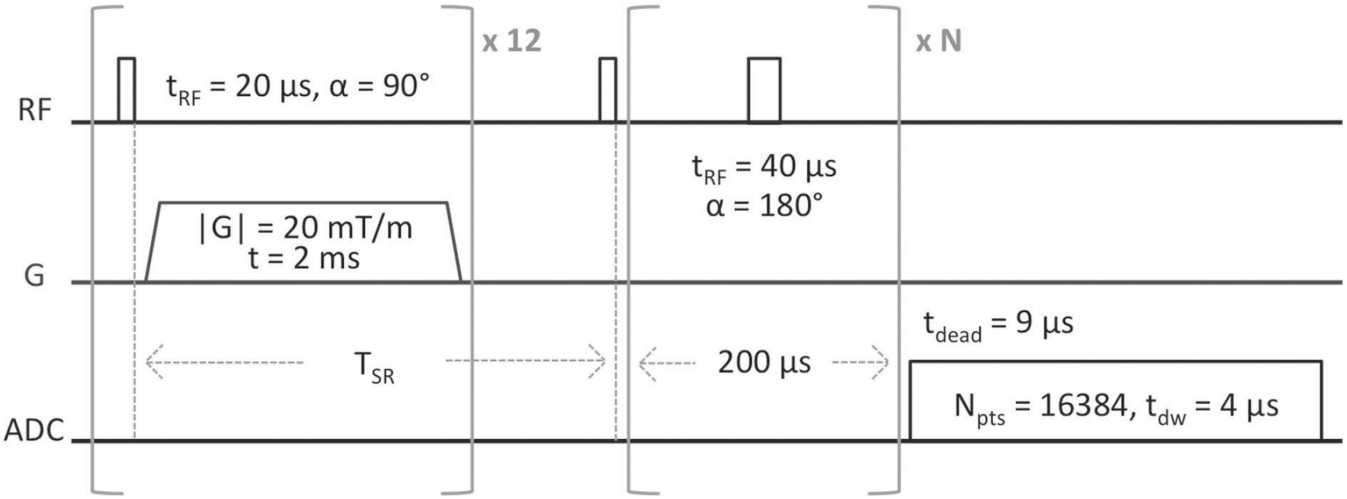

Figure 2.

SR-CPMG pulse sequence. Saturation-recovery times (T_{SR}) were arrayed logarithmically in 12 steps from 3 ms to 6 s, the number of refocusing pulses, N, was arrayed logarithmically from 0 to 5000 in 20 steps, and one signal acquisition was performed.

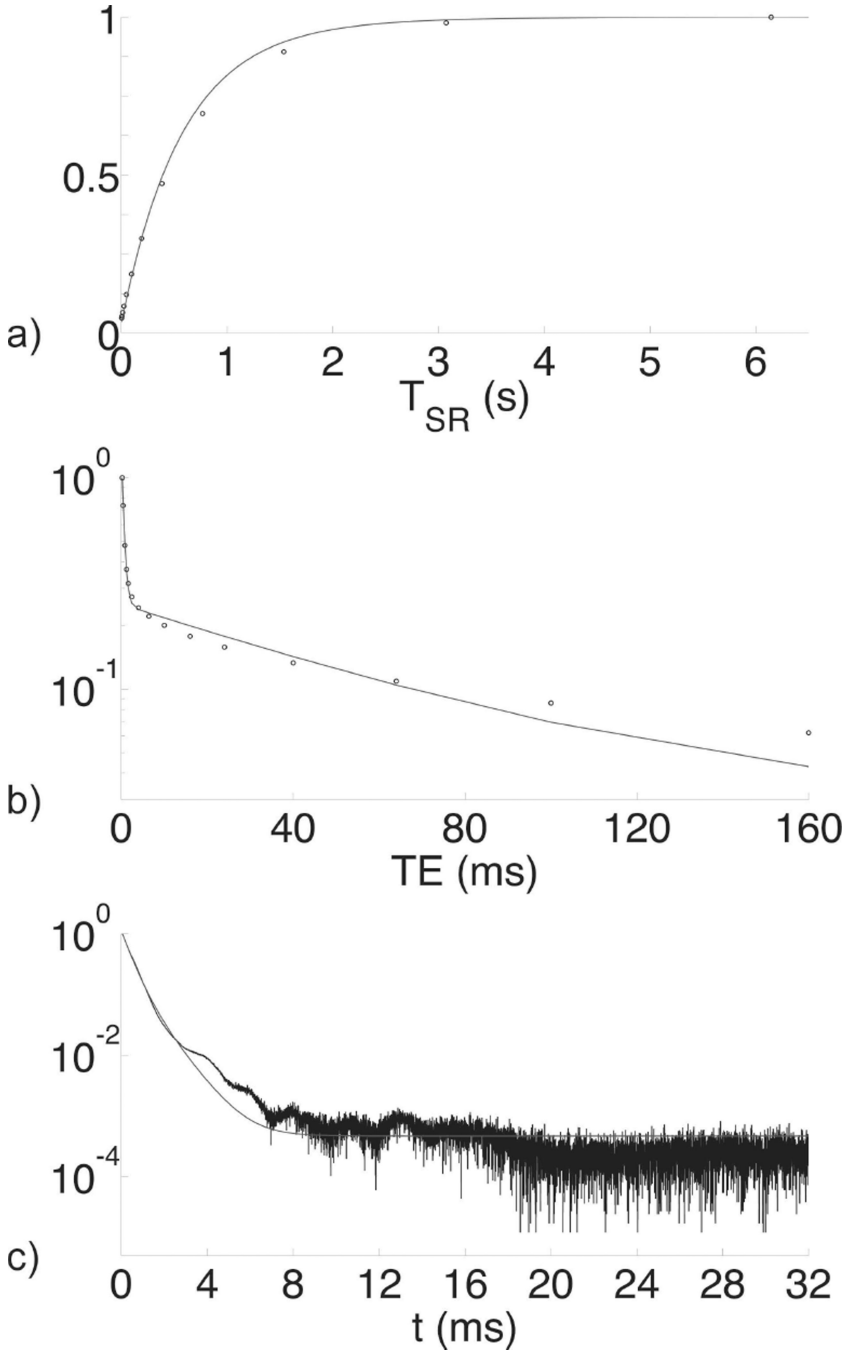

Figure 3.

NMR data (points) from a bone specimen from a 53-year-old male with bi-component fits (curves). Panel (a) shows a T_1 fit of saturation-recovery data, (b) shows a T_2 fit of CPMG echo amplitudes, and (c) shows a T_2* fit of a FID. Although only one-dimensional data are shown, fits were performed using the two-dimensional methods given in the methods section (a,b: T_1–T_2; c: T_2-T_2*). Vertical axes are normalized to M_0.

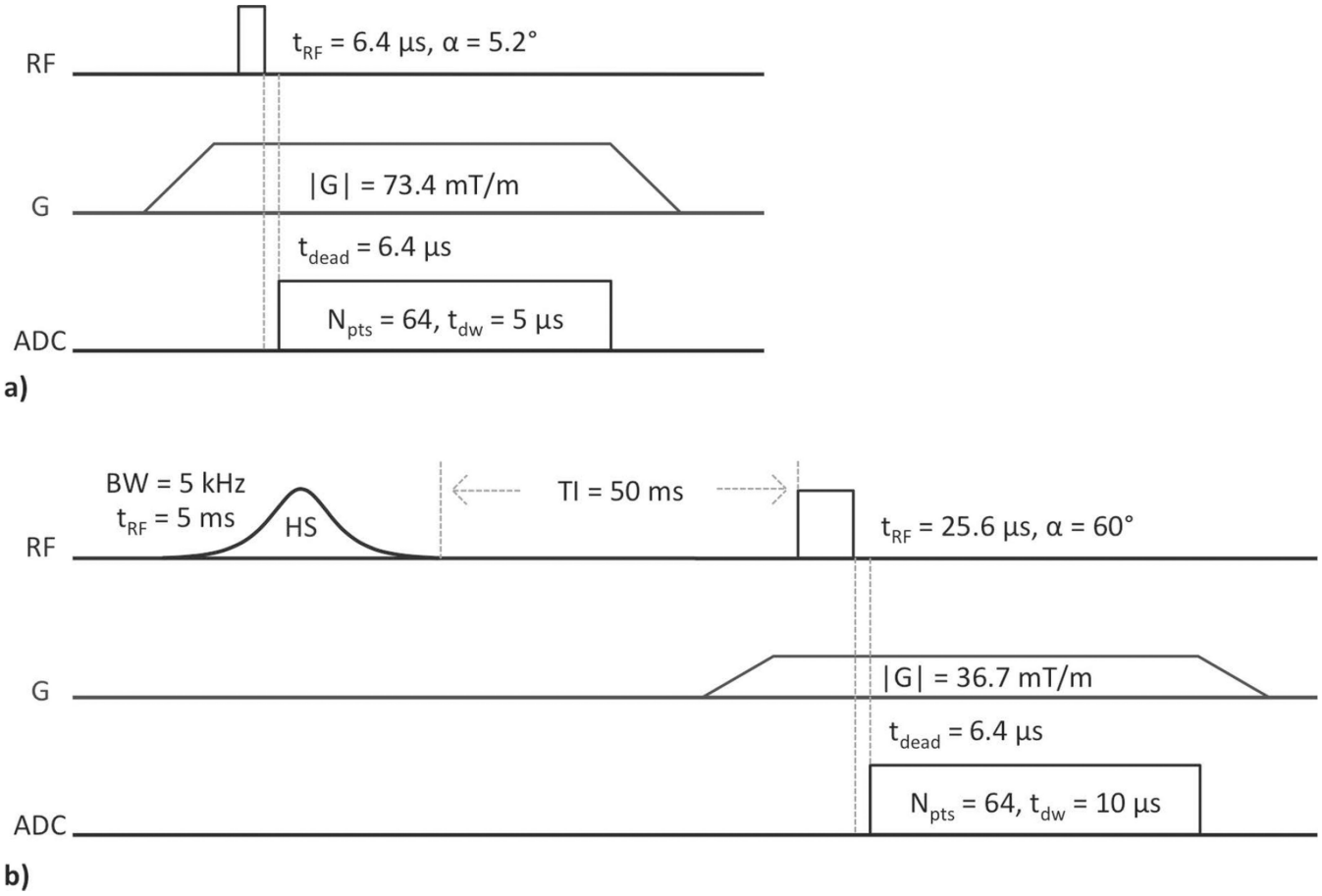

Figure 4.

ZTE (a) and SIR-ZTE (b) imaging pulse sequences. ZTE parameters: 51896 projections, TR = 2 ms, 1 min 43 sec scan time. SIR-ZTE parameters: 6588 projections, TR = 200 ms, 21 min 58 sec scan time. FOV = 64 mm isotropic, resolution = 500 µm isotropic, and 1 signal acquisition for both. The pre-excitation portion of the readout gradient and the short T_2* of bound and pore water ^{1}H signal serve to effectively spoil residual transverse magnetization created by the adiabatic pulse.

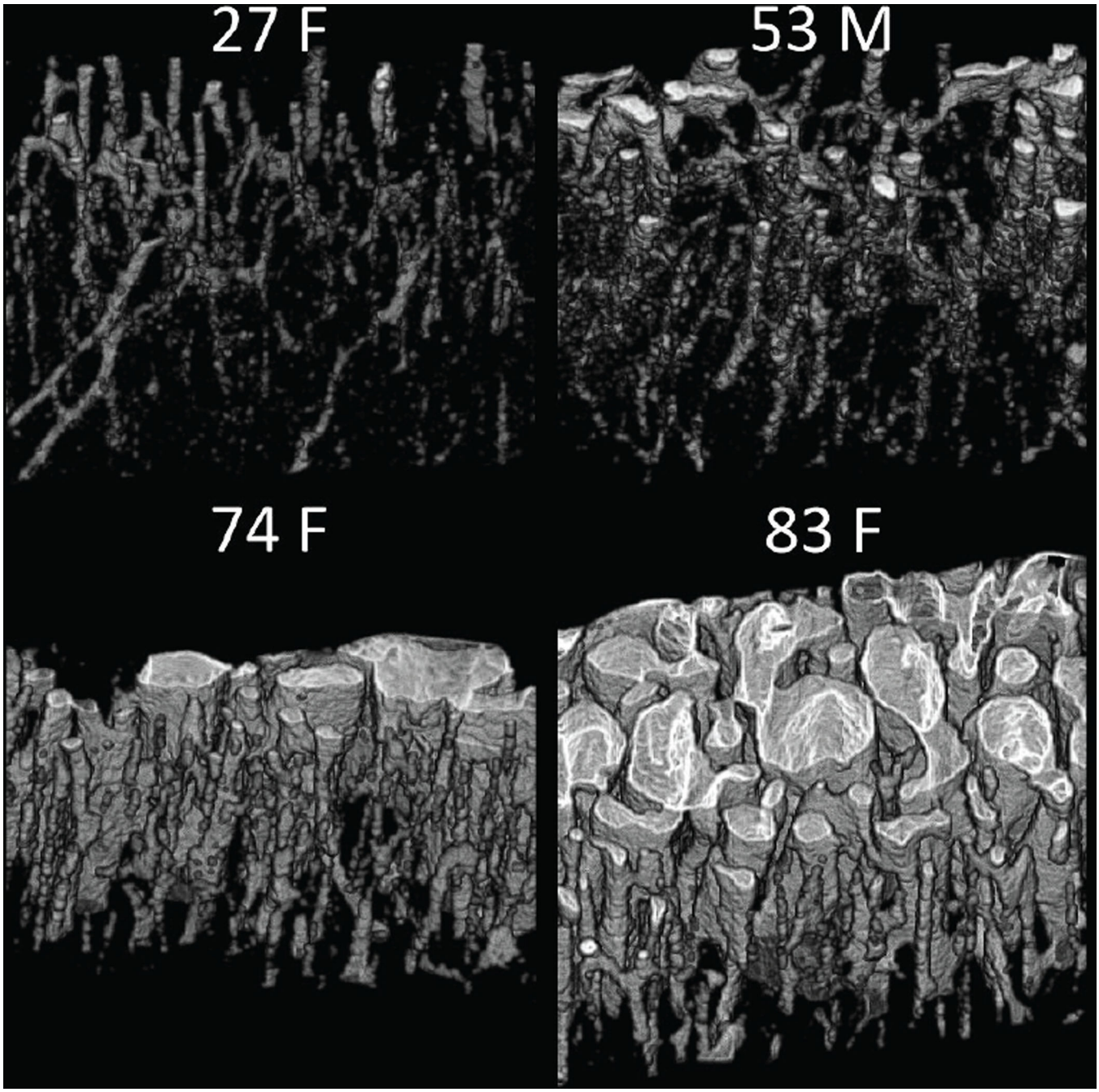

Figure 5.

Volume rendering of the pore spaces (in white) within four representative bone specimens. Note the increased number and size of pores in bone specimens from elderly female donors.

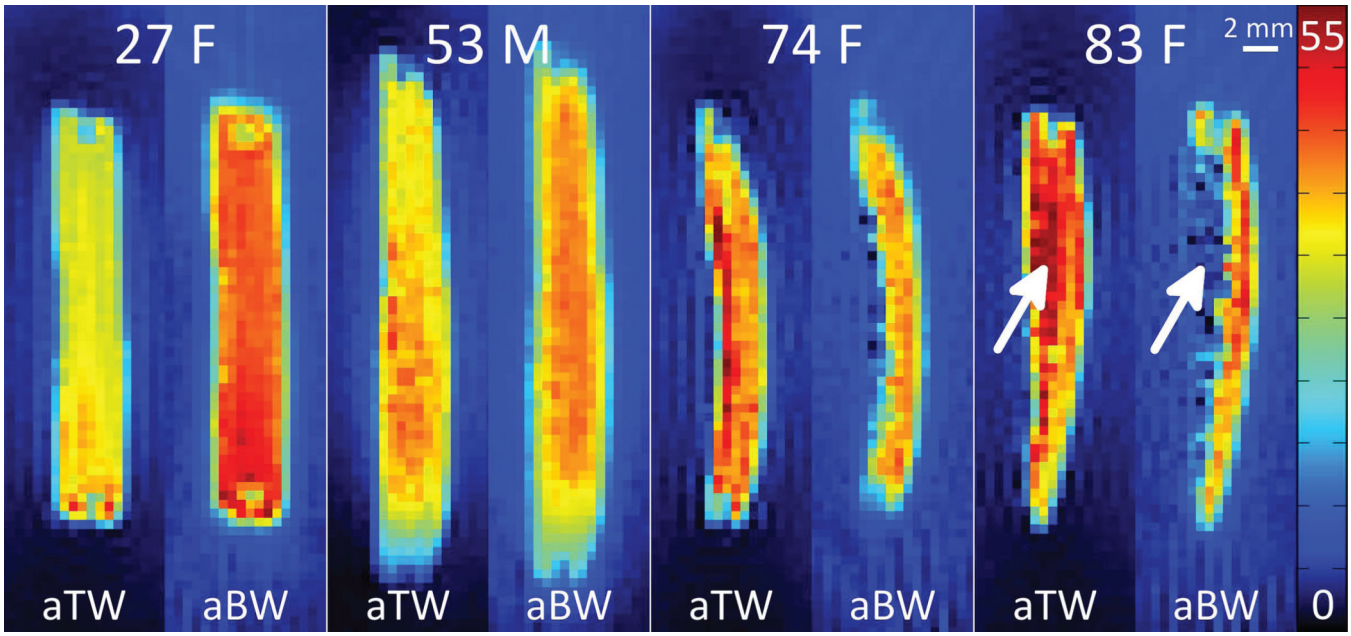

Figure 6.

Maps of apparent total water (aTW) and apparent bound water (aBW) ^{1}H concentrations, in mol/L, in bone specimens from four representative donors. Age and gender of the donors are given within each quadrant, and the endosteal surface of each specimen faces left. Arrows indicate a region of high porosity, which has elevated total water and reduced matrix densities, and correspondingly increased aTW and decreased aBW. Non-zero background signal surrounding the bone specimen arises from extremely short-T_2 signal contributed by the plastic body of the RF probe.

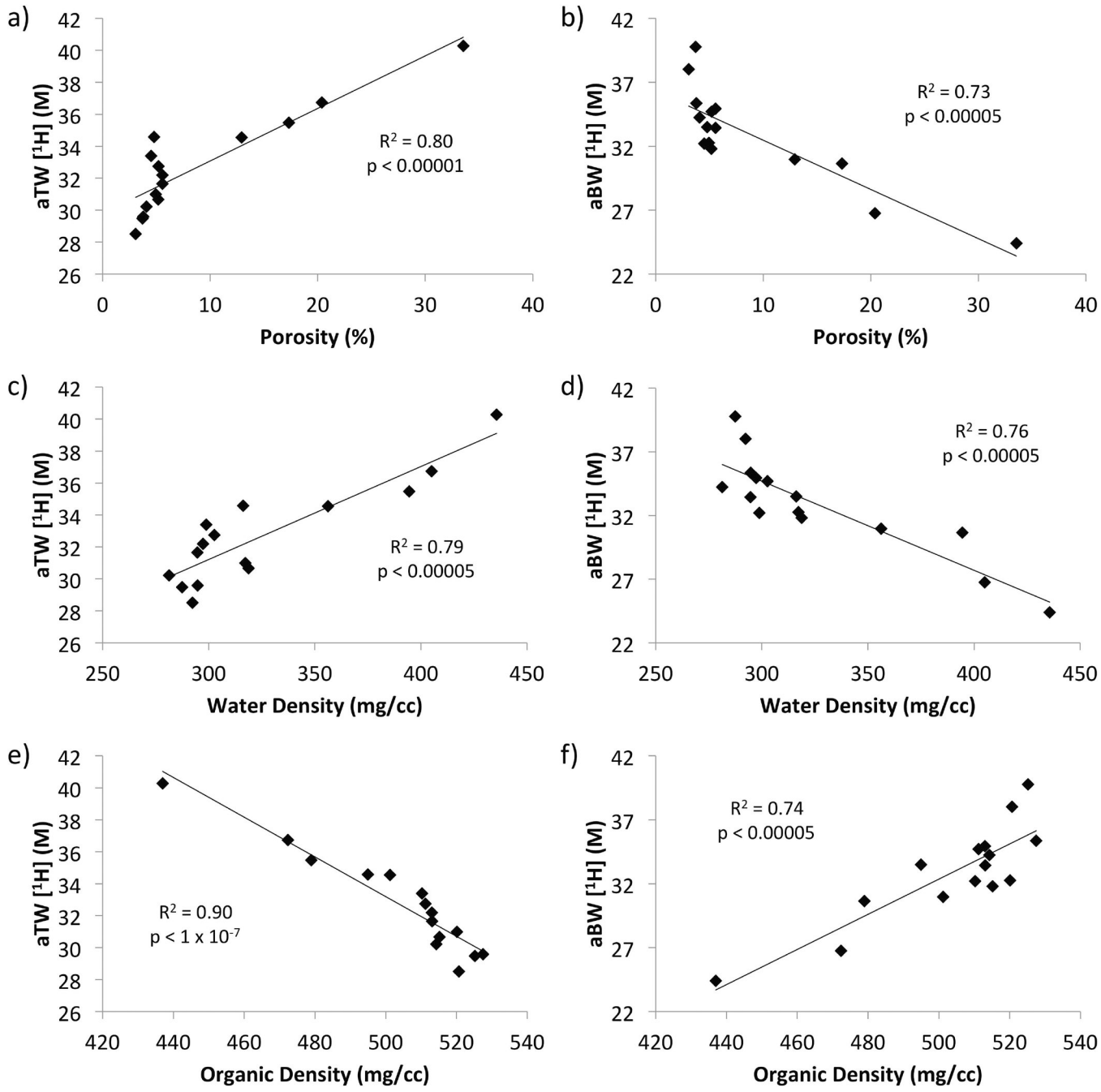

Figure 7.

Scatter plots displaying the correlations of apparent total water (aTW, a,c,e) and apparent bound water (aBW, b,d,f) ^{1}H concentrations versus μCT porosity (a,b), gravimetric water density (c,d), and gravimetric organic matrix density (e,f). Apparent total water ^{1}H concentration is positively correlated with porosity and gravimetric water density and negatively with matrix density, while aBW correlations show the opposite behavior.

Table 1

Apparent total water (aTW) and apparent bound water (aBW) ^{1}H concentration measurements by MRI, and reference measurements by μCT, gravimetry, and ^{1}H NMR. Sample labels indicate age and gender.

Bone	aTW [^{1}H] (M)	aBW [^{1}H] (M)	μCT Porosity (%)	Mineral Density (mg/cc)	Matrix Density (mg/cc)	Water Density (mg/cc)	T_1–T_2 Bound Fraction (%)	Mineralization Mass Ratio	Bone Mineralization (mg/cc)
27F	29.5	39.8	3.70	1197	525.2	287.4	86.6	2.280	1243
30F	28.5	38.0	3.06	1208	520.7	292.3	86.2	2.320	1246
37M	34.6	33.5	4.77	1163	494.9	316.2	78.4	2.351	1222
49M	30.2	34.2	4.08	1207	514.3	281.4	83.8	2.346	1258
53M	31.7	33.4	5.56	1159	513.1	294.6	82.9	2.258	1227
53F	29.6	35.4	3.78	1192	527.5	294.8	86.6	2.260	1239
65F	32.2	34.9	5.57	1161	513.0	297.3	81.2	2.263	1229
69M	32.8	34.7	5.18	1172	511.2	302.7	79.3	2.293	1236
74F	36.7	26.7	20.4	930.7	472.4	405.0	62.4	1.970	1169
75M	33.4	32.2	4.51	1175	510.3	298.8	80.1	2.303	1230
82F	35.5	30.6	17.3	1015	479.0	394.5	66.4	2.119	1227
83F	40.3	24.4	33.5	751.2	437.0	435.6	55.4	1.719	1130
83M	31.0	32.3	4.94	1159	520.1	317.2	77.3	2.228	1219
93M	30.7	31.8	5.18	1219	515.2	318.7	77.6	2.367	1286
97F	34.6	31.0	12.9	1058	501.2	356.2	71.4	2.110	1215
Mean	32.7	32.9	8.96	1118	503.7	326.2	77.0	2.212	1225
StDev	3.2	3.9	8.61	130	24.3	48.4	9.3	0.173	36

Table 2

Inter-parameter correlations (R^2) of measured bone properties. All correlations are statistically significant ($p < 0.05$).

	μCT Porosity (%)	Matrix Density (mg/cc)	Mineral Density (mg/cc)	Water Density (mg/cc)	Mineralization Mass Ratio	Bone Mineralization (mg/cc)	T_1–T_2 Bound Fraction (%)	aBW [^{1}H] (M)
aTW [^{1}H] (M)	0.80	0.90	0.82	0.79	0.69	0.71	0.86	0.77
aBW [^{1}H] (M)	0.73	0.74	0.72	0.76	0.64	0.54	0.86	
T_1–T_2 Bound Fraction (%)	0.90	0.89	0.88	0.96	0.79	0.63		
Bone Mineralization (mg/cc)	0.73	0.70	0.84	0.62	0.84			
Mineralization Mass Ratio	0.94	0.78	0.96	0.82				
Water Density (mg/cc)	0.92	0.86	0.90					
Mineral Density (mg/cc)	0.98	0.91						
Matrix Density (mg/cc)	0.91							